한국해양공학회지 제17권 제2호, pp 1~7, 2003 (ISSN 1225-0767)

Model Parametrization on the Mixing Behavior of Coastal Discharges

JONG-KYU KIM*
*Division of Ocean System, Yosu National University, Yeosu, Korea

KEY WORDS: Mixing Behavior 혼합특성, Coastal Discharges 연안유출수, Buoyancy Flux 부력플럭스, Flow Flux 유동플럭스, Coriolis Force 코리올리력, Bottom Topography 해저지형, Princeton Ocean Model (POM) 해양순환모델

ABSTRACT: *A common feature in the three-dimensional numerical model experiments of coastal discharge with simplified model and idealized external forcings is investigated. The velocity fields due to the buoyancy and flow flux, are spreaded radiately and the surface velocites are much greater than the homegeneous discharges. The coastal dischargd due to the Coriolis force and flow flux are shaped a anticyclical gyre (clockwise) and determined the scale of the gyre in the coastal zone, respectively. The bottom topography restricts a outward extention of the coastal fronts and it accelerates a southward flow.*

1. Introduction

Recently, many coastal areas in the southern part of the Korean peninsula have experienced some problems in water quality, and the environmental efforts to solve it have been conducted. In particular, a vast amount of land-drained material, suspended organic material, industrial waste, and sewage brought onto the coastal ocean regions through river discharge may significantly affect fishery production and water quality. Since pollutants produced by urban and industrial complexes are discharged into the coastal area, the self-purification capacity of seawater in the coastal ocean region has significantly decreased, which poses a serious environmental and social concern. It is important to have a general understanding of the coastal ocean circulation, as well as to trace and predict the pathways and the distributions of river-borne dissolved materials or pollutants in the coastal ocean.

Coastal discharge produces buoyancy-driven flow (large-scale plumes and coastal currents) in coastal ocean regions. When buoyant coastal discharge (river freshwater) is released into a coastal region, occupied by saltier and more dense oceanic water, potential energy becomes available to drive thermo-haline currents, where strong lateral entrainment and vertical mixing occur. Often, the dynamic structure of the spreading low-salinity water over the coastal region is referred to as a coastal (river) plume. Recently, observations and model studies of large-scale buoyant plumes have shown three major types for the horizontal distribution of density (Garvine, 2001). Type 1 represents the typical coastal freshwater plume through observations. The buoyant discharge turns right in the northern hemisphere (downshelf), with the under earth rotation as its source. Type 2 is common in many numerical model studies. Most of the buoyant water at the inlet turns left (upshelf) along the coast to form a continuously growing intrusion. Type 3 turns right, but exhibits a massive anti-cyclic bulge that grows with time; its coastal current is weak, and carries a small fraction of the inlet fresh water or buoyancy flux.

Studies of the temporal and spatial structures of a coastal (river) plume are of considerable interest not only because of their influences on the physical processes of the coastal circulation, but also because of their close relationship to the coastal ecosystem and environmental pollution problems.

The objective of this study is to improve our understanding of the temporal and spatial structures of the coastal discharges and resulting coastal currents and pathways of river-borne material on the coastal ocean region, using the three-dimensional ocean model.

제1저자 김종규 연락처: 전라남도 여수시 둔덕동 산 96-1
061-659-3155 oceaninfo@yosu.ac.kr

2. Numerical Model Experiments

2.1 Three-dimensional numerical model

The Princeton Ocean Model (POM) used here is a three-dimensional, free surface, primitive equation ocean model, which uses the terrain-following sigma coordinate system in the vertical (Blumberg and Mellor, 1987). The numerical scheme used is finite-difference, centered-space in the horizontal, implicit in the vertical, and leapfrog in time. An Asselin filter is used to suppress the numerical noise

(Asselin, 1972). The horizontal grid difference scheme is rendered on an Arakawa C-grid, which is split into a two-dimensional external (depth-integrated/barotropic) mode and a three-dimensional internal (baroclinic) mode, for computing the three velocity components, density, surface elevation, and turbulence parameters. The lateral friction and diffusion terms are calculated by the Smagorinsky (1963) parameterization, while the vertical turbulent mixing is parameterized through the use of the eddy viscosities and diffusivities, calculated according to the level 2.5 turbulence closure scheme (Mellor and Yamada, 1982). POM has been applied to coastal and estuarine regimes, the Gulf Stream, and many other oceanic regions, including semi-enclosed seas, the Medi-terranean Sea, and the South China Sea. Further details concerning the numerics are documented in Blumberg and Mellor (1987), and a description of the model code is given in Mellor (1993).

By assuming an incompressible ocean, the POM solves the following basic equations with two simplifying approximations: hydrostatic and Boussinesq. The continuity equation is:

$$\frac{\partial U}{\partial x} + \frac{\partial V}{\partial y} + \frac{\partial W}{\partial z} = 0 \tag{1}$$

where U, V and W are the horizontal, meridional, and vertical components of the velocity, respectively.

The Reynolds-averaged momentum equations are

$$\frac{\partial U}{\partial t} + U\frac{\partial U}{\partial x} + V\frac{\partial U}{\partial y} + W\frac{\partial U}{\partial z} - fV = -\frac{1}{\rho_0}\frac{\partial P}{\partial x} + \frac{\partial}{\partial z}\left(K_M \frac{\partial U}{\partial z}\right) + F_x \tag{2}$$

$$\frac{\partial V}{\partial t} + U\frac{\partial V}{\partial x} + V\frac{\partial V}{\partial y} + W\frac{\partial V}{\partial z} + fU = -\frac{1}{\rho_0}\frac{\partial P}{\partial y} + \frac{\partial}{\partial z}\left(K_M \frac{\partial V}{\partial z}\right) + F_y \tag{3}$$

$$\rho g = -\frac{\partial P}{\partial z} \tag{4}$$

where ρ_0 and ρ are the reference density and in situ density, respectively; g is the gravitational acceleration, P is the pressure, K_M is the vertical eddy viscosity, f is the Coriolis parameter on the β-plane, and F_x and F_y are the horizontal components of friction.

The conservation equations for temperature and salinity are:

$$\frac{\partial T}{\partial t} + U\frac{\partial T}{\partial x} + V\frac{\partial T}{\partial y} + W\frac{\partial T}{\partial z} = \frac{\partial}{\partial z}\left(K_H \frac{\partial T}{\partial z}\right) + F_T \tag{5}$$

$$\frac{\partial S}{\partial t} + U\frac{\partial S}{\partial x} + V\frac{\partial S}{\partial y} + W\frac{\partial S}{\partial z} = \frac{\partial}{\partial z}\left(K_H \frac{\partial S}{\partial z}\right) + F_S \tag{6}$$

where T is the temperature, S is the salinity, K_H is the vertical eddy diffusivity, and F_T and F_S are the horizontal diffusion terms for heat and salt, respectively.

To better represent realistic bottom topography, the model employs a sigma or terrain-following coordinate system in the vertical, in which local water depths are transformed into a non-dimensional, multi-level system that the vertical coordinate σ ranges from $\sigma = 0$ at $z = \eta$ (at the surface) to $\sigma = -1$ at $z = -H$ (at the bottom) (Phillips, 1957; Blumberg and Mellor, 1987). Thus, the irregular bottom topography is mapped to a flat bottom domain based on the sigma coordinate transformation, which is given as:

$$x^* = x, \quad y^* = y, \quad \sigma = \frac{Z-\eta}{H+\eta}, \quad t^* = t \tag{7}$$

Let the total water depth $D = H + \eta$ and define a new vertical velocity as:

$$w = W - U\left(\sigma\frac{\partial D}{\partial x^*} + \frac{\partial \eta}{\partial x^*}\right) - V\left(\sigma\frac{\partial D}{\partial y^*} + \frac{\partial \eta}{\partial y^*}\right) - \left(\sigma\frac{\partial D}{\partial t^*} + \frac{\partial \eta}{\partial t^*}\right)$$

Physically, the new vertical velocity, w, is the velocity component normal to σ surfaces and satisfies the vertical boundary conditions as:

$$w(x^*, y^*, 0, t^*) = 0, \quad w(x^*, y^*, -1, t^*) = 0$$

The horizontal diffusivities, A_m and A_h are determined according to the Smagorinsky scheme, which can be expressed as:

$$A_m = A_h = C\triangle x \triangle y\left[\left(\frac{\partial U}{\partial x}\right)^2 + \left(\frac{\partial V}{\partial y}\right)^2 + \frac{1}{2}\left(\frac{\partial U}{\partial y} + \frac{\partial V}{\partial x}\right)^2\right]^{1/2}$$

where $\triangle x$ and $\triangle y$ are the horizontal grid size, and C is a non-dimensional parameter, typically in the range of 0.1 to 0.2 in various applications.

POM requires two types of normal velocity: internal and external modes. For the internal mode, the Summerfeld radiation condition has been imposed: while for the external mode, choices of variables are to be specified; either the normal depth-averaged velocity, the surface elevation or their gradients, or a linear combination of these quantities.

2.2 Numerical model experiments

The variations of the coastal circulations, due to the coastal (river) discharge, were simulated using the three-dimensional numerical model (POM, Princeton Ocean Model) in a coastal ocean region. To confirm the effectiveness of flow flux and bottom topography, the simple models were constructed in a coastal ocean region (Fig. 1; Table 1).

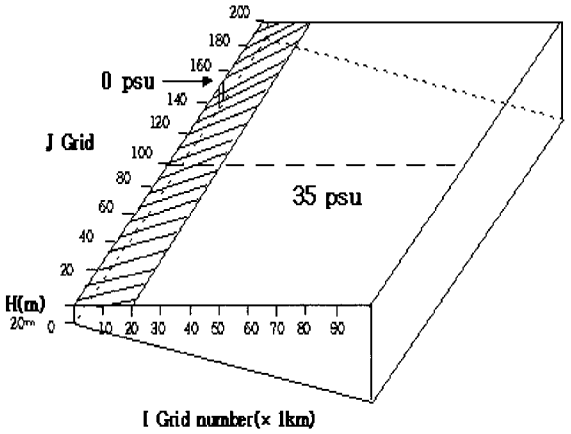

Fig. 1 Schematic configuration of the simple rectangular domain

This model domain consists of 95×200 horizontal cells and 11 vertical levels (Table 1). The horizontal grid is fixed to 1,000m in both x and y directions, and the vertical division on the sigma coordinate is divided to 0.1.

Integration time interval is 10 sec for the external mode and 150 sec for the internal mode. The Coriolis parameter varies with latitude, and all boundaries are closed, except the west and hatching regions, where a radiating boundary condition is used.

Fig. 1 shows the modeled region and its bottom topography. At initialization, salinity is set to 35 psu everywhere except the entrance of inlet, a typical value in this region subject to input from the coastal waters of Korea, and currents to zero.

Table 1 Computational conditions in numerical experiment

Test	Grid spacing	Grid size ($\Delta x=\Delta y$)	Depth (m)	Discharge (m^3/s)	Initial horizontal diffusivity (m^2/s)	DTE (sec)	DTI (sec)	Remarks
1	95×100	1,000 m	20	1,200/6,000	50	10	150	Momentum
2	95×100	1,000 m	20	1,200/6,000	50	10	150	Momentum & Buoyancy
3	95×200	1,000 m	20 & slope=2×10^{-5}	1,200/6,000	50	10	150	Momentum, Buoyancy, Coriolis force

3. Results and Discussion

To better understand and characterize the basic physical mechanism, as well as the formation and evolution, of the coastal discharge under the influence of momentum, buoyancy and flow flux, Coriolis force and bottom topography, the numerical model experiments were designed to investigate the buoyance-driven current in the coastal ocean region. Thus, simplified model and idealized external forcs are applied to investigate the behaviors of coastal discharge in three cases (Table 1). The POM used in this study is described in Blumberg and Mellor (1987). The effect of temperature variations on density was minimal, compared to the effect of salinity.

Fig. 2 shows a typical model result with use of the simple inlet in the case of Test 1 (Table 1). The surface current fields are after 10 days and 5 days of steady force from the inlet flow, due to the momentum and flow flux, respectively. The flow patterns spread in a radial pattern; however, the current speed varies increasingly with the variation of flow flux.

Fig. 3 shows the distribution of surface salinity fields after 10 days of steady force from by the inlet flow, due to the momentum, buoyancy, and flow flux. Fig. 4 shows the distribution of current fields after 10 days of steady force from the inlet flow, due to the momentum, buoyancy, and flow flux. The flow patterns spread in radial pattern in the same representative density currents; while, current speed is faster than that of the homogeneous discharges (Test 1).

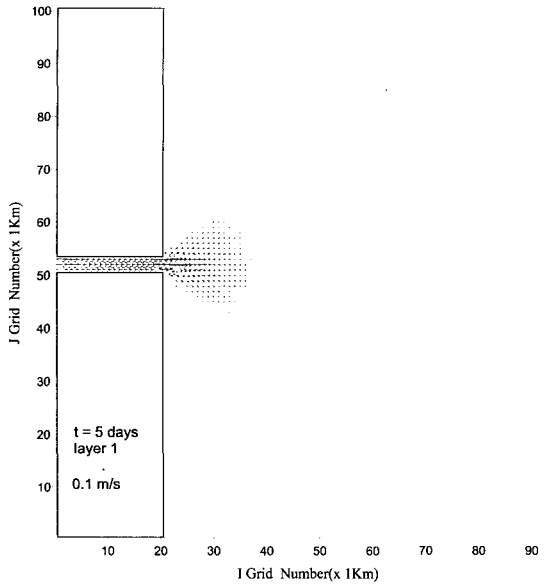

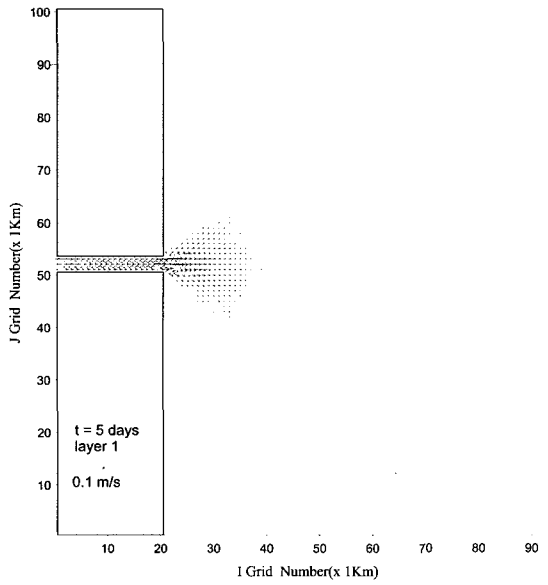

Fig. 2 Surface current fields of the numerical experiment in Test 1 (flow flux : upper=1,200; lower=6,000)

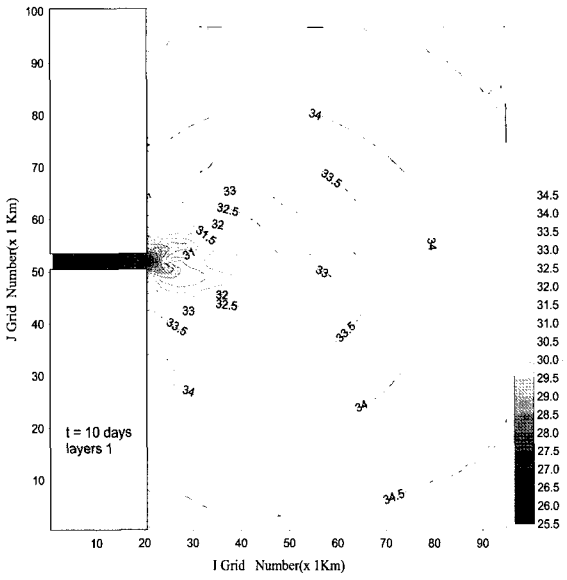

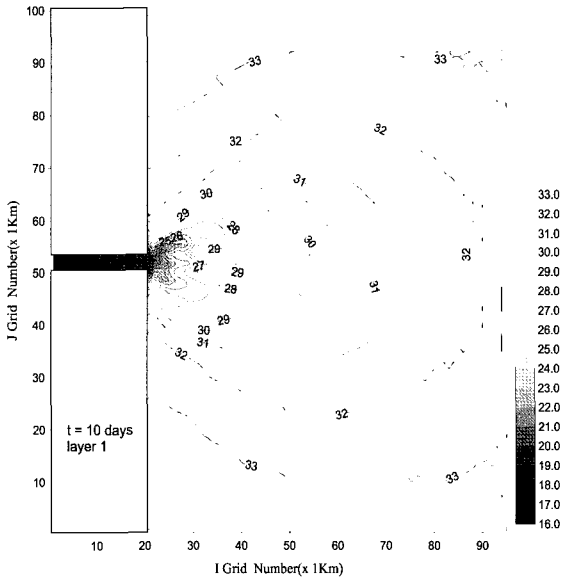

Fig. 3 Surface salinity fields of the numerical experiment in Test 2 (flow flux : upper=1,200; lower=6,000)

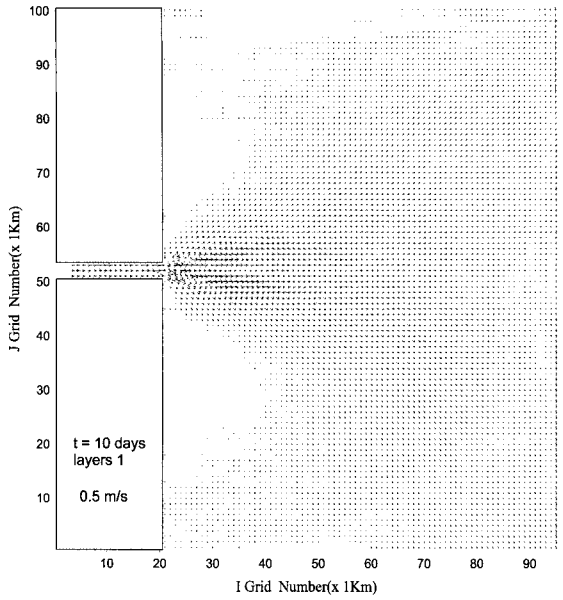

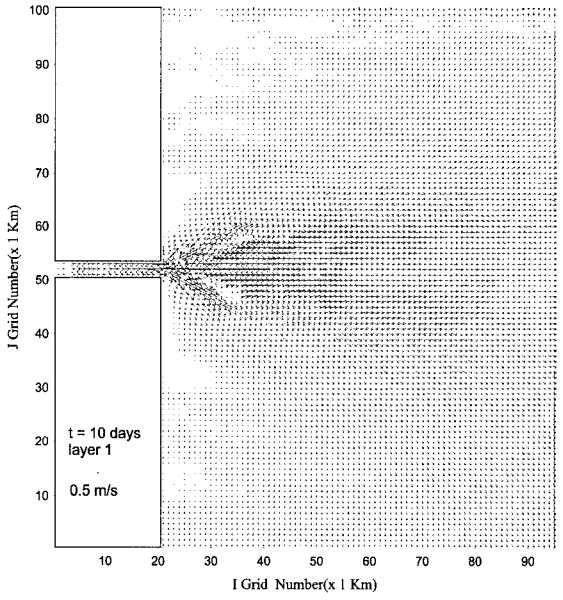

Fig. 4 Current fields of the numerical experiment in Test 2 (flow flux: upper=1,200; lower=6,000)

Fig. 5 shows the non-dimensional parameter of the ratio of current speed at the center of the inflow channel, and the grid points in the experiments of Test 1 and Test 2. The current speed is sensitively to the with buoyancy and flow flux.

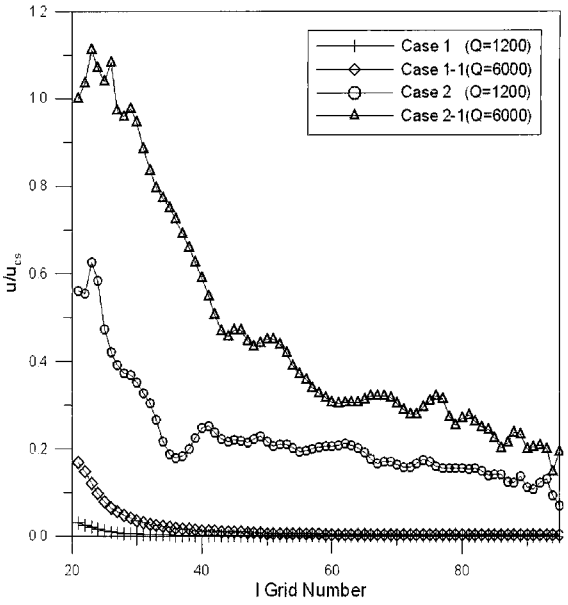

Fig. 5 Ratio of current speed for the center of the inflow channel

Fig. 6 shows the distribution of salinity at the surface and bottom, after 30 days of steady force by the inlet flow, including the effects of momentum, buoyancy, flow flux, and Coriolis force. Due to the Coriolis force, the coastal discharge generates an anti-cyclical gyre (clock-wise) at the front of the inlet mouth, which may be represented by the baroclinic Rossby deformation radius, and is under the equilibrium Coriolis and inertia forces (Fig. 6, upper). The magnitude of the coastal discharges does not affect the structure of the gyre, but does affect the scale of the gyre (Fig. 6, lower).

Fig. 7 shows the distribution of surface salinity after 30 days of steady force from the inlet flow, including the effects of momentum, buoyancy, flow flux, Coriolis force, and bottom topography. In the case of bottom topography more volumes of the coastal discharges are advected to the north, than in the case of flat bottom. The bottom topography restricts an outward extension of the saline fronts and accelerates coastal currents. The development of the northward flow is also a characteristic feature of the coastally-trapped solution of McCreary et al. (1997). This feature is explained as a compensating flow, induced by the southward, flow generated along the density front, which is formed offshore between the low salinity river water and the high salinity coastal ocean water (Bang and Lie, 1999).

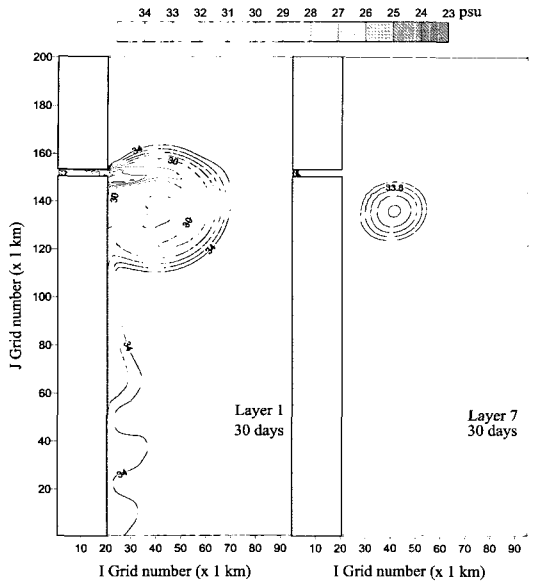

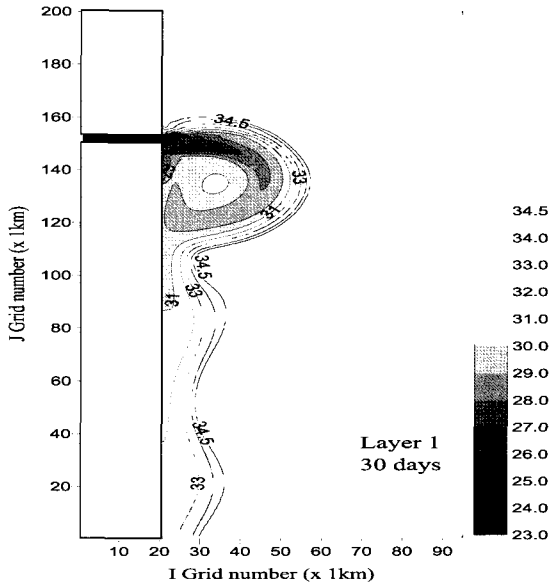

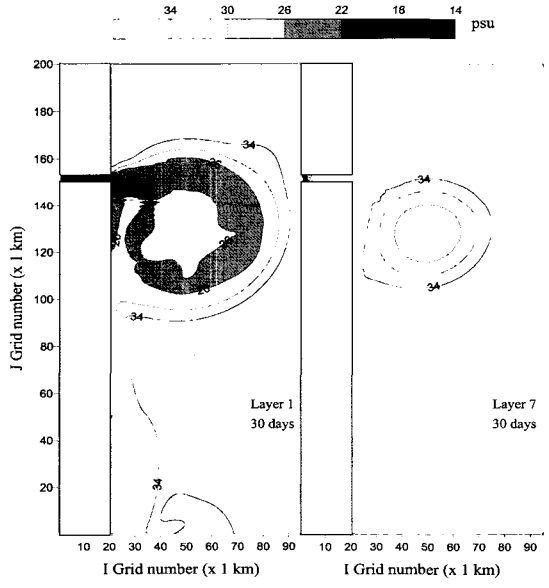

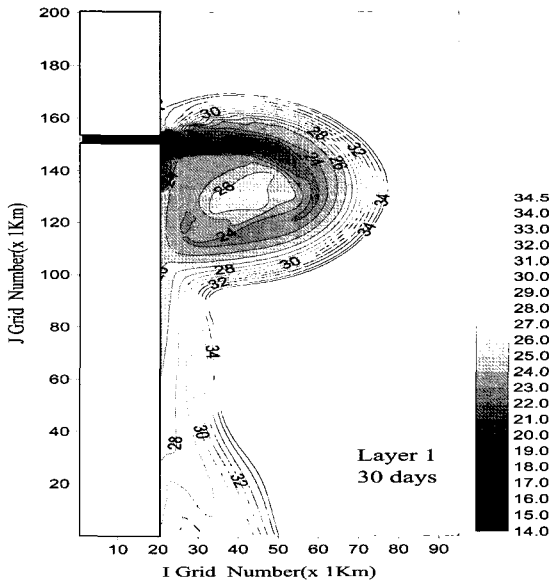

Fig. 6 Surface(left) and bottom(right) salinity fields of the numerical experiment in Test 3 (flow flux: upper=1,200; lower=6,000)

Fig. 7 Surface salinity fields of the numerical experiment with bottom topography in Test 3 (flow flux upper= 1,200; lower=6,000)

Summary and Conclusions

The three-dimensional ocean circulation model experiments on the mixing behaviors of coastal discharge are investigated with the simplified model and idealized external forcings in three cases. However, we do not attempt to compare the problem of realistic model experiments with the observation data. We demonstrate a common feature in numerical model experiments of buoyant coastal discharges with simplified model and idealized external forces. On the other hand, the spreading of buoyant coastal discharge is still possible, and has been observed, in nature. These dynamics can most likely be observed when the discharge has a strong density anomaly and great net transport.

References

Asselin, R. (1972). "Frequency filters for time integrations", Mon. Weather Rev., Vol 100, pp 487-490.

Bang, I.K. and Lie, H.J. (1999). "A numerical experiment on the dispersion of the Changjiang River plume", J. Kor. Soc. Oceanogr., Vol 34, No 4, pp 185-199.

Blumberg., A.F. and Mellor, G.L. (1987). "A description of a three-dimensional coastal ocean circulation model", Three-Dimensional Coastal Ocean Model, N.S. Heaps, ed., Vol 4, American Geophysical Union, Washington, D.C., pp 1-16.

Choi, B.J. (2001). "A study on the mixing behaviors of fresh water discharges using three-dimensional ocean circulation model", MS Thesis, Pukyong National University, pp 59.

Garvine, R.W. (1987). "Estuary plumes and fronts in shelf waters : A layer model", J. Phys. Oceanogr., Vol 17, pp 1877-1896.

Garvine, R.W. (2001). "The impact of model configuration in studies of buoyant coastal discharge", J. Mar. Res., Vol 59, pp 193-225.

Mellor, G.L. (1993). "User's guide for a three-dimensional, primitive equation, numerical ocean model", Princeton NJ 08544-0710, pp 35.

Mellor, G.L. and Yamada, T. (1982). "Development of a turbulence closure model for geophysical fluid problems", Rev. Geophys. Space Phys., Vol 20, pp 851-875.

McCreary, J.P. Jr., Zhang, S. and Shetye, S.R. (1997). "Coastal circulation driven by river outflow in a variable-density 1-layer model", J. Geophys. Res., Vol 102, pp 15,535-15,554.

Phillips, N.A. (1957). "A coordinate system having some special advantages for numerical forecasting", J. Meterol., Vol 14, pp 184-185.

Smagorinsky, J. (1963). "General circulation experiments with the primitive equations, I. The basic experiment", Mon. Weather Rev., Vol 91, pp 16,050-16,064.

2002년 11월 12일 원고 접수
2003년 4월 7일 최종 수정본 채택